True- to sky-blue emitters bearing the thiazolo[5,4-*d*]thiazole electron acceptor for single and tandem organic light-emitting diodes

Abdelaziz Jouaiti,[a,] Dun-Cheng Huang,[b] Valerio Giuso,[c] Cristina Cebrián,[d] Pierluigi Mercandelli,[e] Kuan-Hsun Wang,[b] Chih-Hao Chang,[b,]* and Matteo Mauro[c,]**

[a] Laboratoire de Synthèse et Fonctions des Architectures Moléculaires, UMR7140 Chimie de la Matiere Complexe, Institut Le Bel, Université de Strasbourg & CNRS, 4 rue Blaise, Pascal 67000 Strasbourg (France), e-mail : jouaiti@unistra.fr

[b] Department of Electrical Engineering, Yuan Ze University, Chung-Li, 32003 Taiwan, e-mail: chc@saturn.yzu.edu.tw

[c] Institut de Physique et Chimie des Matériaux de Strasbourg (IPCMS) UMR7504, Université de Strasbourg & CNRS, 23 rue du Loess, 67083 Strasbourg (France), e-mail: mauro@unistra.fr

[d] Laboratoire Lorraine de Chimie Moléculaire (L2CM), Université de Lorraine, CNRS, F-57000 Metz, France

[e] Dipartimento di Chimica, Università degli Studi di Milano, via Camillo Golgi 19, 20133 Milano, Italy

ABSTRACT. A series of emitters displaying efficient photoluminescence and electroluminescence (EL) into the true- to sky-blue region is herein described and employed as electroluminescent materials for the fabrication of efficient blue organic light-emitting diodes (OLEDs). The compounds possess linear, yet twisted, donor-π-acceptor-π-donor (**D**-π-**A**-π-**D**) architecture, where **D** and **A** are a (substituted) carbazole (Cz) and thiazolo[5,4-*d*]thiazole (TzTz) moiety as the electron-donor and accepting unit, respectively. D = 9*H*-carbazol-9-yl and 3,6-di-*tert*-butyl-9*H*-carbazol-9-yl for compound **TzTz-PCz2** and **TzTz-PtbCz2**, respectively. In dilute CH_2Cl_2 solution, both compounds display intense (photoluminescence quantum yield = 60%–74%) and short-lived (τ = *ca.* 0.8–2.0 ns) luminescence arising from an intramolecular charge transfer (^{1}ICT) excited state and falling into the sky-blue to the greenish-blue region (λ_{em} = 448–502 nm). Compared to the previously reported **TzTz-TPA** parental emitter that features two triphenylamine (TPA) donor groups, the highly twisted nature and less extended π-conjugation of the donor-acceptor **TzTz-PCz2** and **TzTz-PtbCz2** counterparts herein presented enable to widen the HOMO-LUMO energy gap and warrant blue shifting of the emission. Finally, OLED devices fabricated by employing the herein proposed emitters are presented as well with both single- and tandem-device architectures. The so-prepared OLEDs display true-blue to sky-blue EL peaking at $\lambda_{EL,max}$ = 460 nm (**TzTz-PCz2**) and 467–470 nm (**TzTz-PtbCz2**) and achieve maximum external quantum efficiency (EQE) and luminance of 10.2% and 44851 cd m^{-2} (for **TzTz-PtbCz2**) in the case of a tandem device, respectively, with mitigated roll-off efficiency. These results demonstrate that the tandem device employing these TzTz donor-acceptor blue emitters raises the feasibility of fluorescent compounds to compete with other potential emitters in practical applications.

KEYWORDS

Blue emitters; density functional theory; donor-acceptor compounds; fluorescence; fused heterocycles; organic light-emitting diodes; thiazolo[5,4-*d*]thiazole.

Introduction

Since the demonstration of the first electroluminescent device based on the organometallic compound aluminum *tris*-quinolinate (Alq_3) described by Tang and VanSlyke,[1] important advances have been achieved in the field of organic light-emitting diodes (OLEDs) from both material and device design point of view.[2-5] In the recent past, OLED technology has reached the market and is currently used mainly in full-color displays applications. Phosphorescent organometallic compounds, and in particular iridium(III)-based complexes, are with no doubt leading emitters with excellent performances in the green to orange/red, and phosphorescent OLEDs (PhOLEDs) fabricated by using thereof have demonstrated outstanding performances in terms of external quantum efficiency (EQE), device lifetime and long-term stability under operating conditions.[6-8] Despite the great efforts made to date, achieving comparable performances in the blue region remains elusive and continues to be a significant issue.[9-13] The long exciton lifetime that typically falls in the few μs regime along with the high triplet exciton energy (E_T >3.0 eV) of blue phosphors favor detrimental quenching phenomena, such as triplet-triplet annihilation and triplet-polaron annihilation. Also, the emitter's chemical decomposition occurs to a much larger extent due to the associated considerable E_T value. As a consequence, severe efficiency roll-off and reduced device lifetime are typically observed in blue PhOLED, particularly when devices are driven at higher current density and brightness. These latter are fundamental requirements for application in lighting technologies, for instance. Overall, these effects still represent severe bottlenecks in OLED device technologies, and several strategies have been proposed to tackle such major challenges.

As far as materials design is concerned, emitters featuring excited states with hybridized local and charge transfer (HLCT) character have been recently proposed. The strategy makes use of

reverse intersystem crossing (rISC) involving the lowest-lying singlet (S_1) and high-lying triplet excited states (T_n, n >1).[14-15] However, the chemical design of materials with properly aligned high-lying singlet and triplet states is far from obvious.

Alternatively, thermally-activated delayed fluorescence (TADF)[16-18] has been proposed as a potential alternative for harvesting triplet excitons and, thus, increasing the theoretical device efficiency up to unity. This approach relies on minimizing the energy splitting between S_1 and T_1 manifolds (namely ΔE_{ST}) and recycling T_1 excitons up to the S_1 manifold through the rISC mechanism. To date, devices with excellent EQE have been demonstrated,[19-23] but achieving high efficiency at higher current density and long-term stability remains a significant challenge in the blue region nowadays owing to the long-lived nature of the delayed emission.

Therefore, fluorescent blue emitters still represent a valuable alternative for achieving robust and highly efficient blue OLEDs. Reaching this goal requires on the one hand the design and investigation of novel materials based on suitable scaffolds for emission in the (deep-)blue region, on the other hand, development of improved device architectures. To date, several classes of compounds have been investigated to this aim,[10-13] but only a minimal number of reports describe the use of emitters bearing the thiazolo[5,4-*d*]thiazole (TzTz) moiety as electroactive material in OLEDs.[24-26] This is in spite of the fact that this scaffold has demonstrated to be of great interest in organic electronics[27-28] as charge transport material in field-effect transistors,[29-32] light-harvesting materials in organic photovoltaics,[33-37] also owing to the excellent redox and optical properties.[38-42]

Herein, the design of novel emitters with linear, yet twisted, donor-π-acceptor-π-donor (**D**-**π**-**A**-**π**-**D**) architecture and containing the TzTz accepting core, namely **TzTz-PCz2** and **TzTz-PbtCz2**, is presented along with their chemical, optical and electroluminescence (EL) characterization. The

compounds feature two peripheral (substituted) carbazole (Cz) units as the electron-donor groups and display intense sky-blue luminescence arising from an intramolecular charge transfer (ICT) excited state. Compared to the previously reported **TzTz-TPA2** parental derivative,[25] which has been used as a benchmark and emits green in thin-film and solid state, the newly proposed emitters display hypsochromically shifted emission falling into the blue to the cyan region with higher photoluminescence quantum yield (PLQY). The optical properties were further elucidated by means of computational analysis employing (time-dependent) density functional theory, namely (TD)-DFT. Finally, the novel compounds were tested as electroluminescent materials in both single- and tandem OLED optimized devices providing true blue to sky-blue EL with satisfactory performances.

Experimental Section

Experimental details concerning syntheses, photophysical techniques, computational methods and OLED devices fabrication can be found in the supplementary method section of the Supporting Information.

Synthesis of TzTz-PCz2 and TzTz-PtbCz2. To a solution of dithiooxamide (0.5 g, 4.15 mmol) in DMF (60 mL) under argon was added the corresponding benzaldehyde, either 4-(9*H*-carbazol-9-yl)benzaldehyde (2.25 g, 8.3 mmol) or 4-[3,6-bis(1,1-dimethylethyl)-9*H*-carbazol-9-yl]benzaldehyde (3.19 g, 8.3 mmol). The mixture was allowed to reflux for 24 hours. Upon cooling, the product was recrystallized out from the resulting solution. The desired compounds were isolated by filtration and purified by washing successively with MeOH, acetone and diethyl ether.

2,5-bis(4-(9*H*-carbazol-9-yl)phenyl)thiazolo[5,4-*d*]thiazole (TzTz-PCz2): yellow solid, 1.16 g, yield 45%. ^{1}H NMR ($CDCl_3$, 500 MHz): δ (ppm) 8.29 (d, *J* = 8 Hz, 4H), 8.18 (d, *J* = 8 Hz, 4H), 7.76 (d, *J* = 8Hz, 4H), 7.54 (d, *J* = 8 Hz, 4H), 7.46 (t, *J* = 8Hz, 4H), 7.33 (t, *J* = 8 Hz, 4H). ^{13}C{^{1}H} NMR ($CDCl_3$, 125 MHz): δ (ppm) 140.4, 139.8, 132.6, 127.9.4, 127.3, 126.1, 123.6, 120.4, 120.3, 109.8. HR-MS (ESI): m/*z* $[M + H]^+$ calcd for $C_{40}H_{25}N_4S_2$ $[M + H]^+$ 625.1515; found 625.1507.

2,5-bis(4-(3,6-di-*tert*-butyl-9*H*-carbazol-9-yl)phenyl)thiazolo[5,4-*d*]thiazole (TzTz-PtbCz2): yellow solid, 1.8 g, yield 51%. ^{1}H NMR ($CDCl_3$, 500 MHz): δ (ppm) 8.22 (d, *J* = 8.5 Hz, 4H), 8.13 (d, *J* = 2 Hz, 4H), 7.71 (d, *J* = 8.5 Hz, 4H), 7.49 (dd, *J* = 2 Hz, *J* = 8 Hz, 4H), 7.44 (d, *J* = 8 Hz, 4H), 1.44 (s, 36H). ^{13}C{^{1}H} NMR ($CDCl_3$, 125 MHz): δ (ppm) 168.3, 151.2, 143.5, 140.5, 138.7, 132.1, 127.9, 126.8, 123.7, 116.4, 109.3, 34.8, 32.0. HR-MS (ESI): m/*z* $[M + H]^+$ calcd for $C_{56}H_{56}N_4S_2$ $[M + H]^+$ 849.4019; found 849.4028.

Results and discussion

Synthesis

Compared to the widely employed triphenylamine (TPA) moiety, carbazole units feature weaker electronic donating ability. Additionally, they possess a combination of high thermal and morphological stability and excellent optical and hole transporting properties: these features make the Cz unit an appealing building block for the preparation of blue-emitting functional materials suitable for optoelectronic devices.

Donor-acceptor type of emitters based on the TzTz accepting core display attractive properties as demonstrated by the archetypal compound **TzTz-TPA2**, but they remain largely unexplored. Aiming at molecular emitters that combine excellent optical with charge-transporting properties suitable for efficient OLED devices, two novel emitters with linear **D-π-A-π-D** architecture were designed by incorporation of electron-donating Cz units, namely **TzTz-PCz2, TzTz-PbtCz2** (see

Scheme 1 for chemical structures), onto the TzTz electron accepting scaffold. Substitution with electron donor units at the 4 position of the two phenyl bridges onto the 2,5-diphenyl-thiazolo[5,4-*d*]thiazole scaffold, namely PhTzTzPh, is indeed expected to mainly stabilize the HOMO, while leaving largely unaffected the LUMO (see also computational section).[43] As a result, the widening of the HOMO-LUMO gap can be envisaged. The compounds were straightforwardly prepared via a double condensation reaction between dithiooxamide and the corresponding aromatic aldehyde in refluxing DMF, as depicted in Scheme 1. ^{1}H and ^{13}C NMR spectroscopy and high-resolution mass spectrometry was employed to fully characterize the products that confirmed the target structures and their suitable purity for further (electro)optical characterization. Chemical characterization data are displayed in Figures S1–S4 of the Supporting Information.

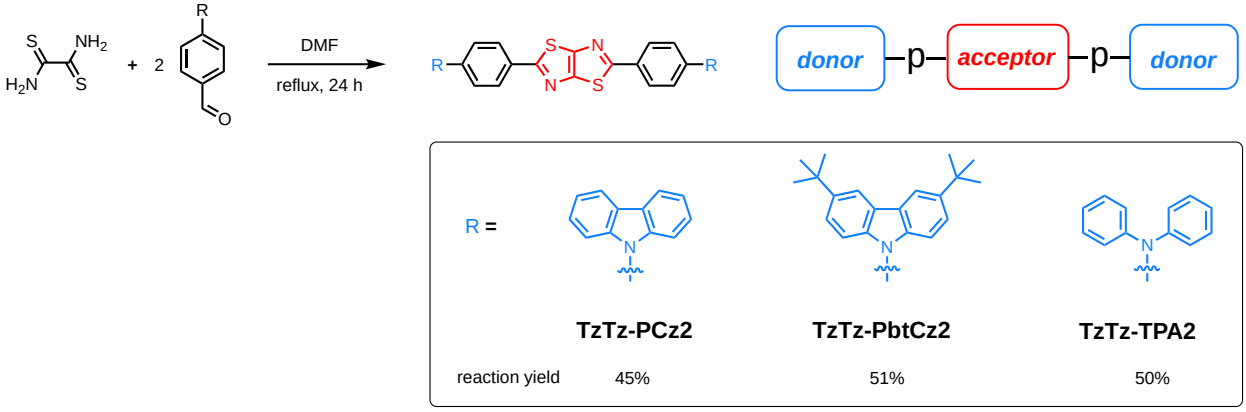

Scheme 1. Schematic synthetic pathway and chemical structure of the three TzTz-based emitters investigated.

Thermal properties

The thermal properties of the three compounds were assessed by thermogravimetric analysis (TGA) and differential scanning calorimetry (DSC) and the corresponding data are plotted in Figures S5–S7 and S8–S10 of the Supporting Information. The decomposition temperatures with

5% weight loss ($T_{5\%}$) are 440°C, 400°C and 400°C for compound **TzTz-PCz2**, **TzTz-PbtCz2** and **TzTz-TPA2**, respectively. The melting point (T_m) of the pristine microcrystalline powders are 342°C and 282°C, for **TzTz-PCz2** and **TzTz-TPA2**, respectively; whereas no melting is observed for **TzTz-PbtCz2** until 300°C where decomposition starts to be significant. These data support that these TzTz-based emitters possess excellent thermal stability and properties, making them suitable candidates for vacuum-processed OLED devices.

Photophysical investigation

Firstly, the photophysical properties of derivatives **TzTz-PCz2, TzTz-PbtCz2** and **TzTz-TPA2** were investigated in dilute (3×10^{-6} M) solution CH_2Cl_2 at room temperature under air. The corresponding UV-Vis absorption and photoluminescence spectra are displayed in Figure 1, and data are summarized in Table 1.

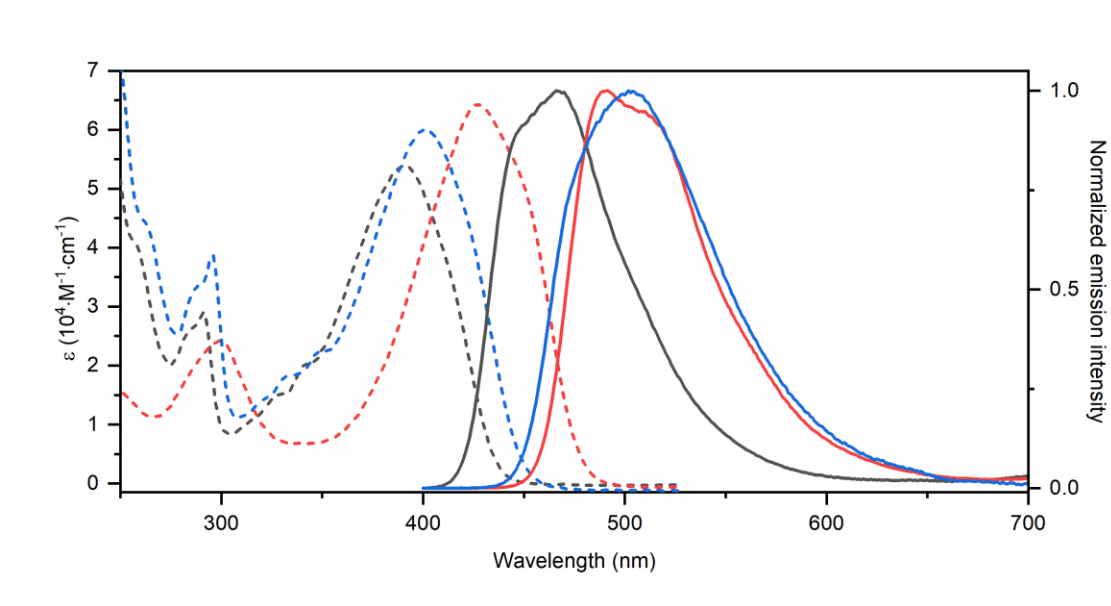

Figure 1. UV-Vis (dashed traces) and photoluminescence (solid traces) spectra of compounds **TzTz-PCz2** (black), **TzTz-PbtCz2** (red) and **TzTz-TPA2** (blue) in CH_2Cl_2 solution at concentration of 3×10^{-6} M. Emission spectra were recorded upon λ_{exc} = 380 nm.

The absorption spectrum is characterized by two bands in the UV region at 260–290 nm that can be attributed to electronic transitions with singlet manifold π–π* character involving the phenyl-carbazole and the thiazolo[5,4-*d*]thiazole scaffold.[43-45] On the other hand, the band at λ_{abs} = 300 nm can be assigned to the triphenylamine fragment for compound **TzTz-TPA2**. At longer wavelengths, the broad, featureless, and more intense ($\varepsilon = 5.4–6.4\times10^4$ M^{-1} cm^{-1}) band in the region λ_{abs} = 400–440 nm results of the overlap of electronic transitions with different character, such as localized excited state (^{1}LE) involving the 2,5-diphenyl-thiazolo[5,4-*d*]thiazole moiety and intramolecular charge-transfer (^{1}ICT) with $\pi_{Cz}\rightarrow\pi^*_{TzTz}$ (for **TzTz-PCz2** / **TzTz-PbtCz2**) and $\pi_{TPA}\rightarrow\pi^*_{TzTz}$ character (for **TzTz-TPA2**). The broad nature of this absorption band is also attributable to the different accessible rotamers along the C–C bond connecting the two phenyls and the thiazolo[5,4-*d*]thiazole central core, as previously observed for related chromophores.[25,43-45] Upon photoexcitation in this lower energy band, CH_2Cl_2 samples display intense blue to cyan photoluminescence with a maximum centered at λ_{em} = 467, 491 and 502 nm, for compound **TzTz-PCz2**, **TzTz-PbtCz2** and **TzTz-TPA2**, respectively, with high intensity, being the PLQY value as high as 0.74, 0.60 and 0.35, respectively. Time-resolved emission curves display mono-exponential decay with observed excited-state lifetimes of 784 ps (**TzTz-PCz2**), 1.98 ns (**TzTz-PbtCz2**) and 991 ps (**TzTz-TPA2)**. These data allow us to estimate the radiative (k_r) and non-radiative (k_{nr}) rate constants that characterize the kinetics of the emissive excited state as follows (see eqns. 1–2):

$$k_r = \text{PLQY} / \tau \qquad \text{eqn. 1}$$

$$k_{nr} = (1 - \text{PLQY}) / \tau \qquad \text{eqn. 2}$$

For all the derivatives, relatively high k_r values in the order of $3.0–9.4\times10^8$ s^{-1} are estimated, characteristic of a strongly allowed radiative process originating from a manifold with mainly singlet character . At this stage, one should notice that photophysical parameters measured for derivative **TzTz-TPA2** differ slightly from those reported elsewhere.[25]

Secondly, the solvent effect was investigated in detail for compound **TzTz-PbtCz2** (see Figure 2). See Table 1 for photophysical data. Variation of the polarity of the solvent does not give rise to a noticeable shift in the absorption spectrum, yet a hypochromic shift of the lower-lying band is observed upon the increase of polarity that could be ascribed to partial aggregation of the chromophores. In sharp contrast, a clear bathochromic shift is observed in the photoluminescence spectra from λ_{em} = 450 to 523 nm when going from less polar toluene to more polar DMSO. This spectral change is accompanied by a variation of the emission band, being structured in toluene with a main vibronic progression of 1300–1500 cm^{-1} attributable to C=C and C=N intramolecular vibrational modes. The band becomes featureless and broader in more polar solvents. Such spectral changes underpin a switch of the nature of the emitting excited state from mainly localized (LE) in toluene to intramolecular charge transfer (ICT) in more polar solvents. Nevertheless, in both toluene and DMSO solvent fitting of the excited-state lifetimes required a bi-exponential model, whereas mono-exponential decays were obtained for samples in the other investigated solvents. This effect could be tentatively ascribed to the modification of the energy landscape yielding to a different population of accessible rotamers that features distinctive radiative processes back to the ground state. As far as samples in acetone are concerned, the addition of trifluoroacetic acid (TFA)

at a concentration of 1 mol L^{-1} decreased the PLQY and the excited state lifetime from 0.07 and 2.86 ns in pure acetone down to 0.01 and 1.40 ns in acetone/TFA (1 mol L^{-1}). This effect is ascribed to a severe quenching of the ICT excited state most likely due to the protonation of the TzTz core at the N sites. Nevertheless, no spectral change in terms of emission band profile and energetics is observed, as depicted in Figure S11, in sharp contrast to what was previously observed for the related compound **TzTz-TPA2**.[25] The emission may be ascribed to residual, unprotonated, emitter molecules in solution.

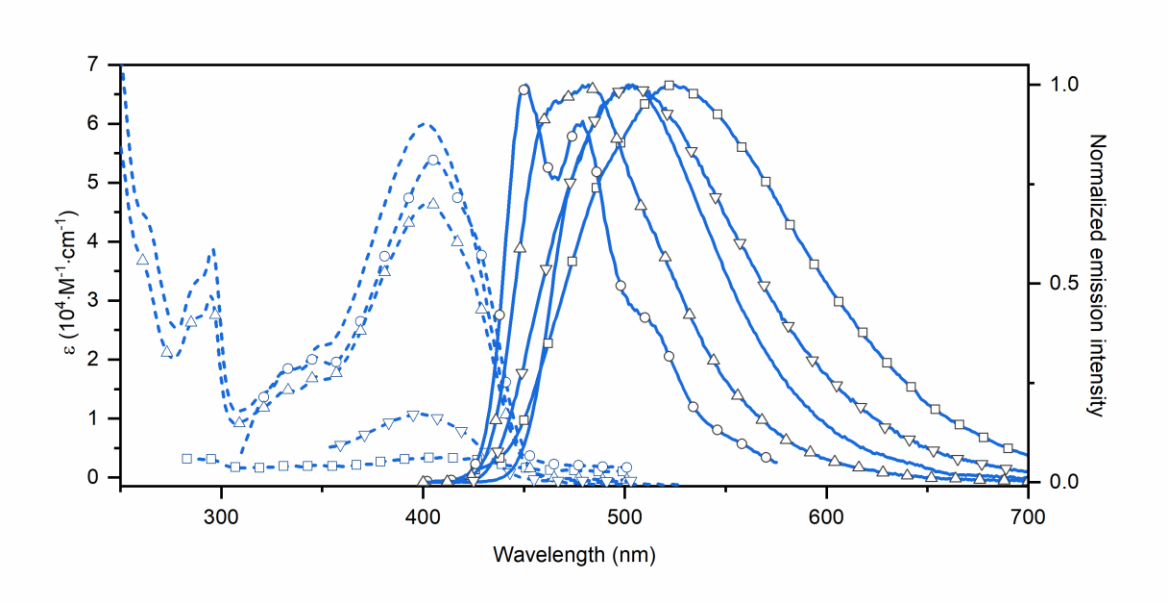

Figure 2. UV-vis (dashed traces) and photoluminescence (solid traces) spectra of compound **TzTz-PbtCz2** recorded at a concentration of 3×10^{-6} M in solvents of various polarity: toluene (round traces), THF (upward triangle traces), CH_2Cl_2 (plain traces), acetone (downward triangle traces) and DMSO (square traces). Emission spectra were recorded upon excitation at λ_{exc} = 300 nm (toluene), 370 nm (DMSO), 380 nm (THF and CH_2Cl_2) and 400 nm (acetone).

The increase in solvent polarity appeared to have little effect on the absorption profile, whereas the emission wavelength was affected to a much larger extent, showing a bathochromic

shift. This observation suggests that environmental effects mainly take place as solvent stabilization affecting the emissive excited state and that a change of the degree of the ICT character from Franck-Condon to a relaxed state might take place. Hence, emission energy was plotted against the solvent orientation polarizability (see Figure 3), following a modified version[46-47] of the Lippert-Mataga relationship (eqn. 3):[48-49]

$$\bar{\nu}_{em} = \frac{2(\mu_e - \mu_g)^2}{hca^3}\left(\frac{\varepsilon_0 - 1}{2\varepsilon_0 + 1} - \frac{n^2 - 1}{2n^2 + 1}\right) + b \qquad \text{eqn. 3}$$

where $\bar{\nu}_{em}$ is the emission in wavenumbers, $(\mu_e - \mu_g)$ is the difference between the excited (μ_e) and ground μ_g state dipole moment, respectively, a is the Onsager radius, h is the Planck's constant, c is the speed of light, the solvent-specific ε_0 and n are the local relative permittivity and refractive index, respectively, and b is the observed emission in the absence of environment-dependent processes. The term Δf defined as by eqn. 4 is called solvent orientation polarizability.

$$\Delta f = \frac{\varepsilon_0 - 1}{2\varepsilon_0 + 1} - \frac{n^2 - 1}{2n^2 + 1} \qquad \text{eqn. 4}$$

Additionally, emission was plotted as a function of the sole relative permittivity component, following eqn. 5 (see Figure 3):

$$\bar{\nu}_{em} = \frac{2(\mu_e - \mu_g)^2}{hca^3}\left(\frac{\varepsilon_0 - 1}{2\varepsilon_0 + 1}\right) + b' \qquad \text{eqn. 5}$$

In both cases, a linear relationship was found with a slope of the regression of *ca.* –12400 and –11600, following eqn. 4 and 6 respectively, which clearly indicates that solvatochromic properties of compound **TzTz-PbtCz2** are mainly influenced by the sole environment dielectric constant. As Supporting Information, a classical Lippert-Mataga plot of the observed Stokes shift is provided in Figure S12 and provides similar linear trends.

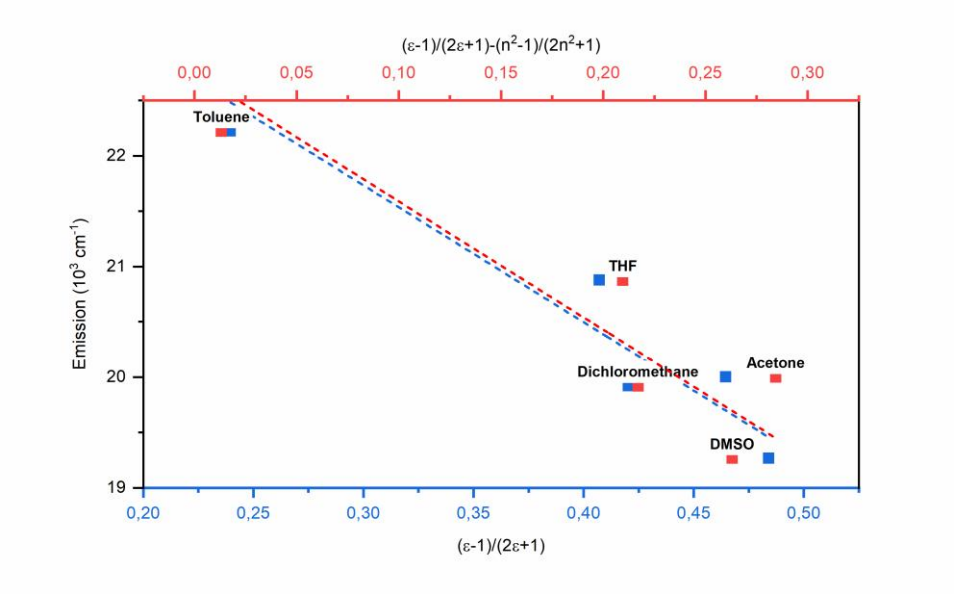

Figure 3. Solvatochromic properties of compound **TzTz-PbtCz2** in solvent of various polarities: plot of the observed emission maximum (in wavenumber) as a function of solvent orientation polarizability, $\Delta f(\varepsilon_0, n)$ (red squares) and solvent permittivity (blue squares) following eqn. 4 and 6, respectively. R^2 value of the fitting are 0.94 (blue trace) and 0.87 (red trace).

Lowering the temperature down to 77 K in a 2-MeTHF glassy matrix causes a hypsochromic shift of the emission profile and an increase of the structural profile compared to the emission in fluid CH_2Cl_2 at room temperature (see Table 2 and Figure S13). In particular, a smaller shift of *ca.* 200 cm^{-1} is observed for compounds **TzTz-PCz2** and **TzTz-TPA2**, whereas compound **TzTz-PbtCz2** displays a more significant variation of about 2100 cm^{-1} in agreement with the larger ICT nature of the emitting excited state that characterizes this latter compound due to the presence of the more donating 3,6-di-*tert*-butyl-carbazolyl moieties. For all the investigated derivatives, time-resolved de-excitation curves could be nicely fitted by single-exponential decays with a lifetime in the range of τ = 1.24–1.48 ns. No long-lived component in either steady-state spectra or time-resolved transient decays could be clearly observed (see Figures S14–S15 of the Supporting

Information). This finding points towards the absence of TADF processes in such class of linear donor-acceptor emitters and lets us describe the radiative process arising from an excited state with admixed ^{1}LE / ^{1}ICT character.

For all the investigated compounds, photoluminescence spectra as solid-state samples in neat powder are displayed in Figure S16 of the Supporting Information. The slight bathochromic shift compared to samples in CH_2Cl_2 solution and the decrease of the PLQY value down to 0.03–0.16 is most likely due to the establishment of intermolecular interactions favored by the large π-conjugated nature of the emitters as well as aggregation-caused quenching phenomena that are at play. Concomitantly, rigidification of the molecular environment in the solid state reduces the rotational conformation freedom and therefore limits rotamers yielding a more structured profile. Nevertheless, it should be pointed out that **TzTz-TPA2** has been shown to display polymorphism with phase-dependent emission properties[50] that are also affected by mechanical triggers.[51] Similar behavior could be expected for carbazole-containing derivatives **TzTz-PCz2** and **TzTz-PbtCz2**, although deeper investigation of their polymorphism is out of the scope of the present work.

Table 1. Photophysical data in dilute (3×10^{-6} M) solution at room temperature under air.

cmpd	medium	$\lambda_{max,abs}$ [nm] (ε [10^4 M^{-1} cm^{-1}])	λ_{em} [nm]	PLQY[a] (%)	lifetime [ps]	k_r [10^8 s^{-1}]	k_{nr} [10^8 s^{-1}]
TzTz-PCz2	CH_2Cl_2	258*sh* (4.04), 284*sh* (2.60) 291 (2.89), 328*sh* (1.50) 340*sh* (1.97), 392 (5.39)	448, 467	74	784	9.44	3.32
TzTz-PbtCz2	Toluene	333*sh* (1.82), 347 (2.03), 405 (5.38), 423*sh* (4.34)	450, 478, 515*sh*	49	360 (16%) 862 (84%)	-	-
	THF	286*sh* (2.66), 295 (3.08), 331 (1.46), 346 (1.69), 401 (4.65)	479	57	1450	3.93	2.97
	acetone	397 (1.08)	500	7	2860	0.24	3.25
	acetone/ TFA (1M)	397 (1.11)	500	1	1400	0.03	3.46
	CH_2Cl_2	263*sh* (4.39), 287*sh* (3.29), 296 (3.87), 332*sh* (1.81), 348*sh* (2.22), 401 (5.99)	502	60	1980	3.03	2.02
	DMSO	407 (0.33)	523	4	3.43 ns (85%) 5.50 ns (15%)	-	-
TzTz-TPA2	CH_2Cl_2	300 (2.42), 427 (6.42), 447*sh* (5.53)	491, 515*sh*	35	991	3.56	6.56

sh denotes a shoulder; [a] $E_{0,0}$ is an estimated optical bandgap determined as the crossing point between the absorption and emission spectra.

Table 2. Photophysical data in 2-MeTHF glassy matrix at 77 K and solid state at room temperature.

cmpd	*medium*	λ_{em} [nm]	lifetime [ps]	PLQY (%)
TzTz-PCz2	*77 K*	444, 466, 500	1240	-
	solid state	519*sh*, 543, 582, 631*sh*	609 (36%) 1610 (59%)	16
TzTz-PbtCz2	*77 K*	454, 480, 513, 550	1390	-
	solid state	492, 520, 559*sh*	314 (65%) 831 (35%)	7
TzTz-TPA2	*77 K*	486, 517, 556, 602	1480	-
	solid state	526, 571	132 (77%) 420 (23%)	3

sh denotes a shoulder.

Computational study

To shed a better light onto their photophysical and electronic features, compounds **TzTz-PCz2**, **TzTz-PbtCz2**, and **TzTz-TPA2** were investigated computationally in the frame of DFT and TD-DFT calculations. It should be nevertheless pointed out that these molecules are characterized by a relatively large degree of conformational freedom due to the rotation about the bonds that connect the aromatic rings. Additional freedom is provided by the rotation of the *tert*-butyl substituents with respect to the carbazole moieties. In the following discussion, only results obtained for the more stable conformer of each species will be presented.

As observed in the solid-state structure determined for the unsubstituted molecule,[52] the 2,5-diphenylthiazolothiazole fragment appears to be nearly planar in all optimized species. Conversely, the *N*-carbazolyl and *N*,*N*-diphenylamine substituents are prevented from being coplanar with the PhTzTzPh scaffold due to interactions involving the *ortho*-hydrogen atoms of the aromatic rings. The dihedral angle between the planes defined by the *N*-carbazolyl and phenyl rings is quite similar in the two species **TzTz-PCz2** and **TzTz-PbtCz2**, being its value of 51.3 and 49.4° respectively, while such angle decreases to 31.2° for **TzTz-TPA2** yielding to a more planar architecture.

Computations show that the frontier molecular orbitals of the three species correspond to the aromatic (HOMO) and quinoid (LUMO) structures of the diphenylthiazolothiazole core (see Figure 4). In particular, the LUMO is localized on the PhTzTzPh core mainly, with a limited contribution from the *N*-carbazolyl or the *N*,*N*-diphenylamino substituents (5.5, 5.9, and 10.4% for **TzTz-PCz2**, **TzTz-PbtCz2**, and **TzTz-TPA2**, respectively). On the contrary, as previously observed for the analogous pyridine-substituted species,[43] the HOMO is substantially delocalized over the substituents (59.4, 66.9, and 50.2% for **TzTz-PCz2**, **TzTz-PbtCz2**, and **TzTz-TPA2**,

respectively). When compared to the unsubstituted PhTzTzPh benchmark compound, destabilization of HOMO and narrowing of the HOMO–LUMO energy gap is computed for the three species (see Table 3).

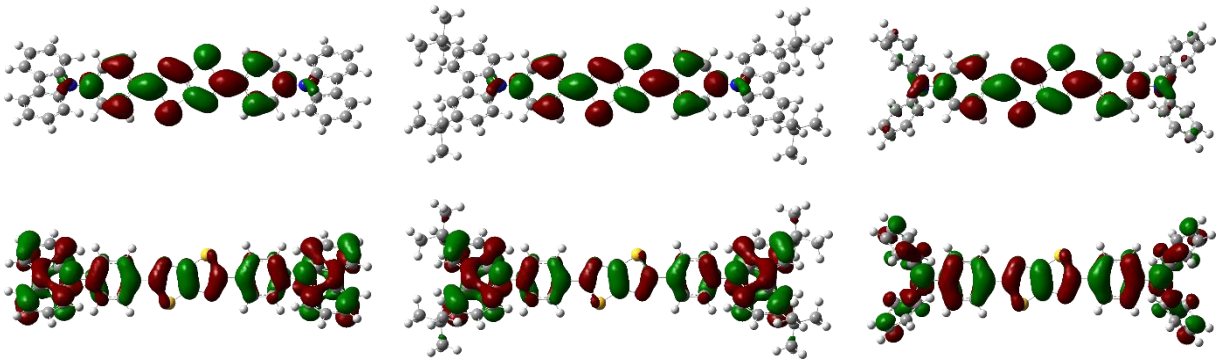

TzTz-PCz2 **TzTz-PbtCz2** **TzTz-TPA2**

Figure 4. Isodensity surface plots for the HOMO (lower row) and LUMO (upper row) of **TzTz-PCz2**, **TzTz-PbtCz2**, and **TzTz-TPA2**.

Table 3. Energy for the HOMO and LUMO levels and HOMO-LUMO gap computed for the derivative **TzTz-PCz2**, **TzTz-PbtCz2**, and **TzTz-TPA2**. The data obtained for the unsubstituted PhTzTzPh is also listed for comparison.

	E_{HOMO} [eV]	E_{LUMO} [eV]	E_g [eV]
TzTz-PCz2	–5.670	–2.202	3.469
TzTz-PbtCz2	–5.534	–2.169	3.365
TzTz-TPA2	–5.173	–1.924	3.250
PhTzTzPh	–6.042	–2.027	4.015

A broad $S_0 \rightarrow S_1$ excitation dominates the absorption spectrum of these species at low energy with HOMO–LUMO character. This transition is computed at 431, 445 and 467 nm for **TzTz-PCz2**, **TzTz-PbtCz2**, and **TzTz-TPA2**, respectively. The corresponding electron density-

difference maps (EDDMs) for the three molecules are depicted in Figure S17, showing how the transition involves a redistribution of the electron density extended all over the molecule and not limited to the TzTz core. In particular, the charge transfer from the substituents to the PhTzTzPh core computed for the three species amounts to 0.357, 0.404, and 0.244 e^- for **TzTz-PCz2**, **TzTz-PbtCz2**, and **TzTz-TPA2**, respectively. As previously reported for similar species,[45] the presence of many different rotamers and the low energy required for the vibration around bonds connecting the constituting rings can be considered responsible for the broad appearance of the absorption peak, taking into account that variations in dihedral angles affect differently the HOMO and LUMO energy and lead to variation in the corresponding excitation energy. In accordance with the results already reported for similar *para*-substituted species and for the parent compound PhTzTzPh, the oscillator strength computed for the HOMO–LUMO excitation is much larger than that of any other excitation down to 250 nm.

Due to the enhanced quinoid character of the lowest-lying singlet excited state (S_1) computed for these molecules, the typical altered alternation of short and long bond lengths can be found in their optimized S_1 geometry. The EDDMs calculated for the emission $S_1 \rightarrow S_0$ are very similar to those calculated for the absorption, allowing to draw similar conclusion. Both vertical and adiabatic energies have been computed for the $S_1 \rightarrow S_0$ transition. Energetic values computed by means of these two approaches are quite different (*ca.* 0.20 eV) as expected, due to the substantial geometrical difference between the lowest-lying singlet excited (S_1) and ground (S_0) state. Overall, calculated values slightly underestimate the emission energies observed experimentally, yet the trend is well reproduced for the three species (see Figure 5). The emission spectrum of **TzTz-PbtCz2** computed in toluene shows a vibrational structure that can be quite well simulated according to the Franck-Condon principle. As expected for a transition mainly involving the TzTz

core, the vibronic structure of the band is mainly determined by the stretching of the C–C and C–N bonds of the thiazothiazole moiety (ν_{250} at 1485 cm^{-1}).

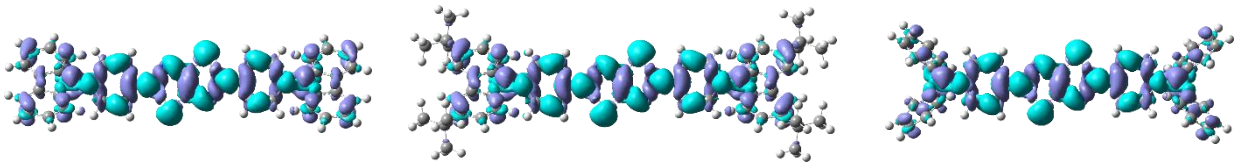

ΔE = 2.379 (*2.600*) eV	ΔE = 2.338 (*2.540*) eV	ΔE = 2.199 (*2.388*) eV
λ = 521 (*477*) nm	λ = 530 (*488*) nm	λ = 564 (*519*) nm
TzTz-PCz2	**TzTz-PbtCz2**	**TzTz-TPA2**

Figure 5. EDDMs computed (at the optimized S_1 geometry) for the vertical transition $S_1 \rightarrow S_0$ of **TzTz-PCz2**, **TzTz-PbtCz2**, and **TzTz-TPA2**. Energy computed for the corresponding adiabatic transition is also reported (*in italics*). Decrease and increase in electron density is indicated with cyan and violet contour, respectively.

OLED devices

These fluorescent compounds were then used as emitters for the device tests. As the compounds have different energy bandgaps, the host materials and corresponding carrier transport materials need to be tuned to exert their properties. Therefore, we designed two device architectures for blue-emitting **TzTz-PCz2** and **TzTz-PbtCz2** and green-emitting **TzTz-TPA2**. Considering the carrier transport and energy transfer, we selected bipolar *N*,*N*'-dicarbazolyl-3,5-benzene (mCP) as the host material for the synthesized blue emitters [53], meanwhile, bipolar 4,4′-bis(*N*-carbazolyl)-1,1′-biphenyl (CBP) with a lower energy bandgap was used for the green emitter.[54] In addition, since the high-energy excitons would form on the blue emitters, carrier transport materials must have a wide energy bandgap to prevent exciton migration or diffusion.

Thus, 1,3,5-tri[(3-pyridyl)-phen-3-yl]benzene (TmPyPB) was chosen as the electron transport layer (ETL) due to its high electron mobility and wide energy bandgap [55]. On the other hand, considering the HOMO energy level matching, di-[4-(*N,N*-ditolylamino)-phenyl]cyclohexane (TAPC) and 4,4′,4″-*tris*(carbazol-9-yl)-triphenylamine (TCTA) were combined to form a stepwise hole transport layer (HTL) in both sets of devices [56]. The thickness of each layer and the emitter concentrations were carefully regulated to maximize efficiency. For instance, Figure S18 shows **TzTz-PbtCz2**-based devices with different doping concentrations, and the results indicated that the optimized doping concentration is 8 weight percent. Consequently, the device architecture for the blue-emitting OLEDs (*i.e.*, devices A and B) was set to ITO (120 nm)/TAPC (30 nm)/TCTA (10 nm)/mCP doped with 8 wt.% dopant (30 nm)/TmPyPB (50 nm)/LiF (0.8 nm)/Al (120 nm), where the LiF and aluminum were respectively used as the electron injection layer and the cathode. As for the green-emitting device, the energy of exciton is slightly lower than that of blue emitters mentioned above. Hence, a simpler device architecture with a single HTL using TAPC was adopted, while the ETL selected bis-4,6-(3,5-di-3-pyridylphenyl)-2-methylpyrimidine (B3PyMPM) because of its adequate energy bandgap and electron mobility [57]. Consequently, the green-emitting device C is configured as ITO (120 nm) /TAPC (40 nm)/CBP doped with 8 wt.% dopant (30 nm)/B3PyMPM (50 nm)/LiF (0.8 nm)/Al (120 nm). Figure 6 depicts the chemical structures of all the employed materials and the schematic architecture of the fabricated OLEDs.

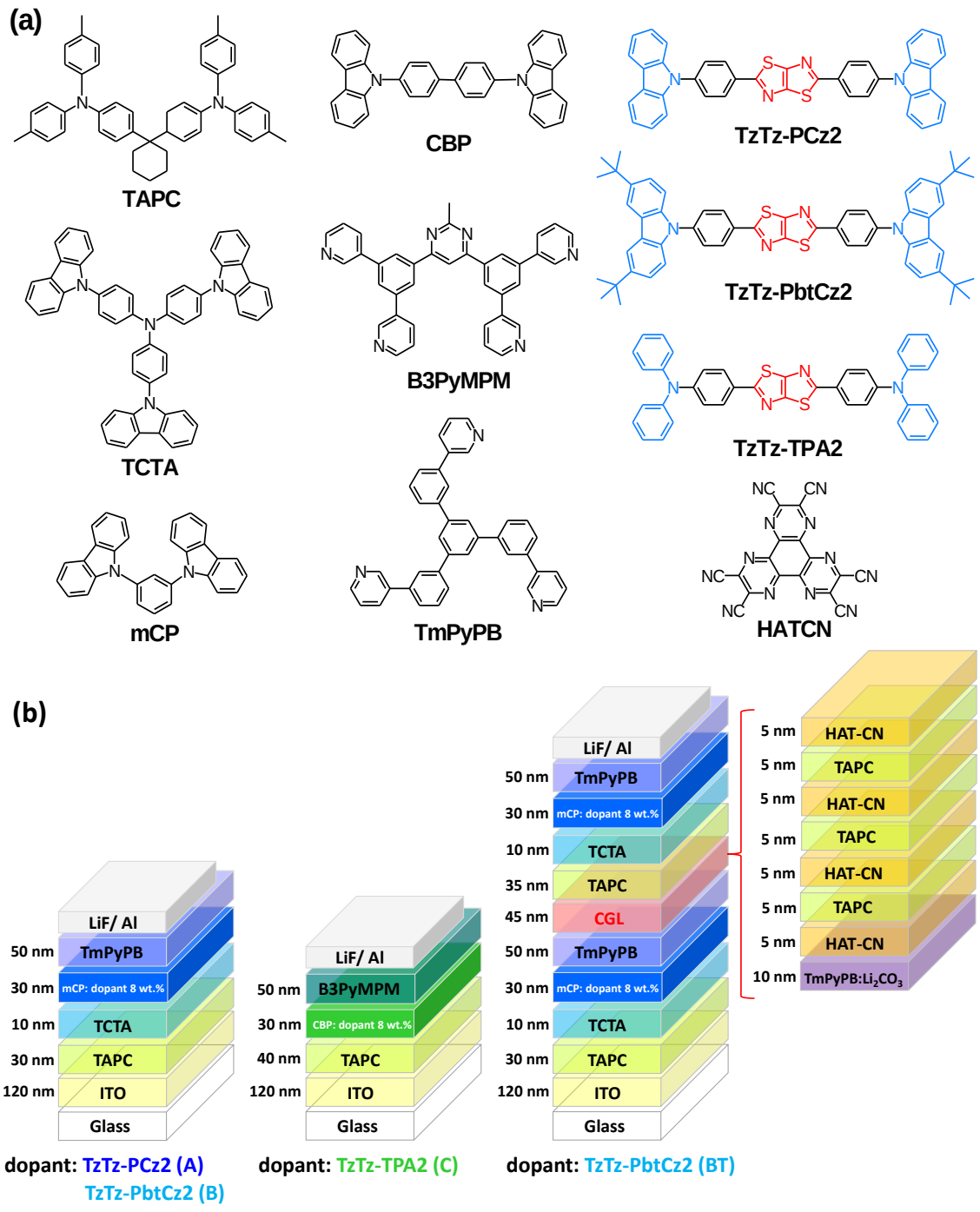

Figure 6. (a) Structural drawings of the materials used in OLEDs; (b) schematic structures of the fabricated OLEDs with different emitters.

Figure 7 and Table 4 respectively show the corresponding electroluminescence characteristics and numerical data. As shown in Figure 7a, the EL spectra of devices A, B, and C were similar to the respective photoluminescence (PL) spectra of the emitters measured in toluene, showing that the exciton formed on the dopant only. In addition, the energy was effectively transferred from the host to the guest in both the blue-emitting and green-emitting devices, and the exciton was well confined within the EML [58]. From the current density–voltage (*J–V*) curves shown in Figure 7b, device C showed a much lower turn-on voltage of 2.6 V compared to those of devices A and B, due to the simpler device architecture as well as the smaller energy bandgaps of the host-guest system. Nevertheless, devices A and B present a higher current density at high voltage ranges, indicating better carrier transport capability or a lower possibility of carrier trapping. As shown in Figure 7c, the luminance levels of the devices follow the trends of C > B > A. Devices A, B, and C respectively reached maximum luminance values of 21122, 36806, and 53990 cd m^{-2}. This is because human eyes respond more strongly to green emissions [59]; hence, the true-blue-emitting and the sky-blue-emitting devices (*i.e.*, A and B) produced a lower luminance than the green-emitting device C. Figures 7d, 7e, and 7f respectively depict the external quantum efficiency (EQE), luminance efficiency, and power efficiency curves versus luminance. The maximum efficiencies of devices A, B, and C respectively reached 4.4% (8.3 cd A^{-1} and 7.2 lm W^{-1}), 5.3% (10.7 cd A^{-1} and 9.3 lm W^{-1}), and 6.9% (20.8 cd A^{-1} and 25.2 lm W^{-1}). Considering that only 25% of singlet excitons were harvested, the high EL efficiency obtained using these **TzTz**-based fluorescent compounds implies their high quantum yields and the carrier balance approximately achieved in this device structure. At a higher practical luminance of 10^2 cd m^{-2}, the EQE values of devices A−C presented efficiency drops by 6.8%, 17.0%, and 20.3% of their respective peak values

in comparison to those recorded at 10^2 cd m^{-2}. The mitigated efficiency roll-off obtained in these devices reflects the excellence of these **TzTz**-based fluorescent compounds in EL applications.

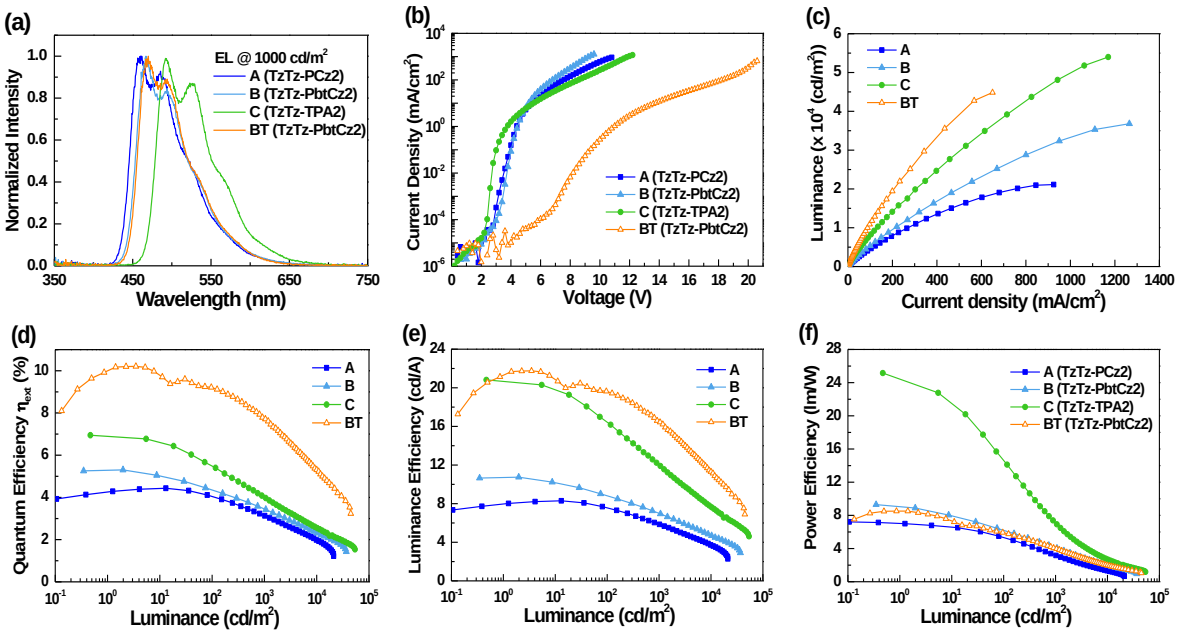

Figure 7. (a) Normalized EL spectra at a luminance of 10^3 cd m^{-2}; (b) current density−voltage (*J*−*V*) characteristics; (c) luminance−current density (*L*−*J*) characteristics; (d) external quantum efficiency vs luminance; (e) luminance efficiency vs luminance; (f) power efficiency vs luminance for devices A, B, C, and BT.

The tandem device structure is proposed to fulfill the requirements of a qualified display or lighting source with abundant luminance and high efficiency. A typical tandem device consists of several individual emission units (EUs) connected by charge generation layers (CGLs) that can improve device efficiency depending on the quantity of EL units [60]. Herein, device B's maximum efficiency and brightness levels indicate that **TzTz-PbtCz2** has a high potential for use in blue devices, making it suitable for the fabrication of tandem devices for practical applications. An electron-transporting TmPyPB doped with Li_2CO_3 was used as the *n*-type layer to facilitate

electron injection into the pure TmPyPB ETL of the first EU [61]. The core CGL was constructed by combining an *n*-type 1,4,5,8,9,11-hexaazatriphenylene-hexacarbonitrile (HAT-CN) and a *p*-type TAPC, where the *n*-type layer/*p*-type layer structure could be considered an organic heterojunction (OHJ) pair [62]. HAT-CN has a strong oxidizing property, while TAPC possesses a low ionization potential, leading to a small energy bandgap between the LUMO of HAT-CN and the HOMO of TAPC and thus enhancing the hole-electron generation and separation at the interface. Furthermore, based on the results demonstrated by Ma's group, the quantity of OHJ pairs could be increased to boost the current density and thus improve the carrier balance in both EUs [63]. The outcomes of the experiments with varied OHJ pairs indicate that the performance of the tandem device could be optimized by adopting four OHJ pairs in the CGL structures, as shown in Figure S19 and Table S1. Consequently, Figure 6 shows an optimal tandem device fabricated with the following generalized design: ITO (120 nm)/TAPC (30 nm)/TCTA (10 nm)/mCP doped with 8 wt.% **TzTz-PbtCz2** (30 nm)/TmPyPB (40 nm)/TmPyPB doped with Li_2CO_3 10 wt.% (10 nm)/HAT-CN (5 nm)/TAPC (5 nm)/ HAT-CN (5 nm)/TAPC (5 nm)/ HAT-CN (5 nm)/TAPC (5 nm)/ HAT-CN (5 nm)/TAPC (35 nm)/TCTA (10 nm)/mCP doped with 8 wt.% **TzTz-PbtCz2** (30 nm)/TmPyPB (50 nm)/LiF (0.8 nm)/Al (120 nm). The EL characteristics and the corresponding numeric data of the tandem device BT are also depicted in Figure 7 and Table 2.

As shown in Figure 7a, the EL spectral profile of device BT was similar to that of device B with a single EU, illustrating the slight influence of the complicated tandem device architecture. The *J-V* curves in Figure 7b show that the tandem device with two EUs needs more than twice the operating voltage of device B. Taking the current density of 600 mA cm^{-2} as an example, the respective luminance values of devices B and BT achieved 23156 and 43589 cd m^{-2}, a nearly 1.9-fold increase. Moreover, as shown in Figures 7d, 7e, and 7f, the tandem device BT presented a

much higher peak efficiency of 10.2% (21.8 cd/A and 8.5 lm/W). The peak EQE of device BT was also about 1.9 times that of device B. In addition, the EQE values of device BT presented efficiency drops of 9.8% from the respective peak value compared to that recorded at 10^2 cd m^{-2}, which was much smaller than that of device B. These results demonstrate that the tandem device raises the feasibility of fluorescent compounds to compete with other potential emitters in practical applications.

Table 4. EL characteristics of tested devices with different fluorescent emitters.

Device		**A**	**B**	**C**	**BT**
Architecture		Single EU			Double EUs
Emitter		**TzTz-PCz2**	**TzTz-PbtCz2**	**TzTz-TPA2**	**TzTz-PbtCz2**
Host		mCP	mCP	CBP	mCP
External Quantum Efficiency (%)	[a]	4.4	5.3	6.9	10.2
	[b]	4.1	4.4	5.5	9.2
Luminance Efficiency (cd A^{-1})	[a]	8.3	10.7	20.8	21.8
	[b]	7.6	8.9	16.5	19.6
Power Efficiency (lm W^{-1})	[a]	7.2	9.3	25.2	8.5
	[b]	5.4	6.2	14.7	5.9
V_{on} (V)	[c]	3.5	3.7	2.6	7.9
λ_{peak} (nm)	[d]	460	467	492	470
Max Luminance (cd m^{-2}) [V]		21122 [10.8]	36806 [9.6]	53990 [12.2]	44851 [20.6]
	[b]	(0.17, 0.27)	(0.18, 0.32)	(0.25, 0.56)	(0.18, 0.32)

CIE1931 coordinates (x, y)	[d]	(0.17, 0.27)	(0.17, 0.31)	(0.25, 0.55)	(0.17, 0.31)

[a] Maximum efficiency; [b] measured at 10^2 cd m^{-2}; [c] turn-on voltage measured at 1 cd m^{-2}; measured at 10^3 cd m^{-2}.

Conclusions

The molecular chemical design and optical properties of a novel series of symmetric blue electroluminescent compounds with linear **D**-π-**A**-π-**D** architecture were presented in detail. Introduction of (substituted) carbazolyl donor moieties that also possess good hole transporting characteristics allowed to increase the degree of twisting about each of the two **D**-π-**A** bonds and enabled the widening of the HOMO–LUMO energy gap, as also supported by computational (TD)-DFT analysis. As a consequence, sky-blue to greenish-blue photoluminescence with high efficiency is observed in dilute CH_2Cl_2 solution arising from an excited state with ^{1}ICT character. Overall, these features promoted the use of these new emitters as electroluminescent materials in single and tandem OLED devices. Optimization of the device architectures allowed satisfactory EL performances, including true- to sky-blue EL ($\lambda_{em,max}$ = 460–470 nm) with peak EQE, luminance efficiency, and maximum luminance as high as 10.2%, 19.6 cd A^{-1}, and 44851 cd m^{-2}, respectively. Finally, these results demonstrate that emitters based on the underexplored TzTz electron-accepting unit are a suitable scaffold for the preparation of efficient PL and EL materials with blue emission and that the tandem device employing these TzTz donor-acceptor blue emitters raises the feasibility of fluorescent compounds to compete with other potential emitters in practical applications. Expansion of the chemical diversity of these TzTz emitters is currently ongoing in order to further push the emission spectra deeper into the blue.

ASSOCIATED CONTENT

The following files are available free of charge.

Chemical characterization of the new compounds including ^{1}H and $^{13}C\{^{1}H\}$ NMR spectra, HR-ESI-MS spectra, thermal analysis, supplementary photophysical, computational and OLED device data (PDF)

Cartesian coordinated of the optimized structures (.xyz file format)

AUTHOR INFORMATION

Corresponding Author

* E-mail: jouaiti@unistra.fr (A.J.)

* E-mail: mauro@unistra.fr (M.M.)

* E-mail: chc@saturn.yzu.edu.tw (C.-H.C.)

Author Contributions

The manuscript was written through contributions of all authors. All authors have given approval to the final version of the manuscript.

Funding Sources

The Université de Strasbourg and the CNRS are kindly acknowledged for financial support. M.M. gratefully acknowledges the French Agence Nationale de Recherche (ANR) for funding the grants ANR-18-CE06-007-01 “SoftAction”, ANR-20-CE29-0021 “PhotoMecha”, ANR-21-CE29-0015 “ChirON”. M.M. and A.J. acknowledge the generous funding provided by the ANR-22-CE07-0049-02 “BoostOLED” grant. The College Doctoral of the Université de Strasbourg for partially funding the PhD fellowship of V.G. C.-H.C gratefully acknowledges the funding support from the

National Science and Technology Council of Taiwan, under the grant number (MOST 110-2221-E-155-033-MY2, 111-2221-E-155-012-MY2, and NSTC 112-2923-E-155-002-MY4).

ACKNOWLEDGMENT

M.M. and V.G. acknowledge the help offered by Robin Fleischel of the UFR de Mathématique et d'Informatique of the Université de Strasbourg with coding and data processing. Dr. Benoît Heinrich is kindly acknowledged for performing the thermal analysis.

REFERENCES

(1) Tang, C. W.; VanSlyke, S. A. Organic Electroluminescent Diodes. *Appl. Phys. Lett.* **1987**, *51*, 913–915. https://doi.org/10.1063/1.98799.

(2) Tao, Y.; Yuan, K.; Chen, T.; Xu, P.; Li, H.; Chen, R.; Zheng, C.; Zhang, L.; Huang, W. Thermally Activated Delayed Fluorescence Materials Towards the Breakthrough of Organoelectronics. *Adv. Mater.* **2014**, *26*, 7931–7958. https://doi.org/10.1002/adma.201402532.

(3) Hong, G.; Gan, X.; Leonhardt, C.; Zhang, Z.; Seibert, J.; Busch, J. M.; Bräse, S. A Brief History of OLEDs—Emitter Development and Industry Milestones. *Adv. Mater.* **2021**, *33*, 2005630. https://doi.org/10.1002/adma.202005630.

(4) Volz, D.; Wallesch, M.; Fléchon, C.; Danz, M.; Verma, A.; Navarro, J. M.; Zink, D. M.; Bräse, S.; Baumann, T. From Iridium and Platinum to Copper and Carbon: New Avenues for More Sustainability in Organic Light-Emitting Diodes. *Green Chem.* **2015**, *17*, 1988–2011. https://doi.org/10.1039/c4gc02195a.

(5) Nakanotani, H.; Higuchi, T.; Furukawa, T.; Masui, K.; Morimoto, K.; Numata, M.; Tanaka, H.; Sagara, Y.; Yasuda, T.; Adachi, C. High-Efficiency Organic Light-Emitting Diodes with Fluorescent Emitters. *Nat. Commun.* **2014**, *5*, 4016. https://doi.org/10.1038/ncomms5016.

(6) Armaroli, N.; Bolink, H.J. (Eds.) *Photoluminescent Materials and Electroluminescent Devices*, Springer, 2017, vol. 374, pp. 1-395.

(7) Chi, Y.; Chang, T.-K.; Ganesan, P.; Rajakannu, P. Emissive Bis-Tridentate Ir(III) Metal Complexes: Tactics, Photophysics and Applications. *Coord. Chem. Rev.* **2017**, *346*, 91–100. https://doi.org/10.1016/j.ccr.2016.11.016.

(8) Czerwieniec, R.; Leitl, M. J.; Homeier, H. H. H.; Yersin, H. Cu(I) Complexes – Thermally Activated Delayed Fluorescence. Photophysical Approach and Material Design. *Coord. Chem. Rev.* **2016**, *325*, 2–28. https://doi.org/10.1016/j.ccr.2016.06.016.

(9) Lee, J.; Chen, H.-F.; Batagoda, T.; Coburn, C.; Djurovich, P. I.; Thompson, M. E.; Forrest, S. R. Deep Blue Phosphorescent Organic Light-Emitting Diodes with Very High Brightness and Efficiency. *Nature Mater.* **2016**, *15*, 92–98. https://doi.org/10.1038/nmat4446.

(10) Yang, X.; Xu, X.; Zhou, G. Recent Advances of the Emitters for High Performance Deep-Blue Organic Light-Emitting Diodes. *J. Mater. Chem. C* **2015**, *3*, 913–944. https://doi.org/10.1039/c4tc02474e.

(11) Im, Y.; Byun, S. Y.; Kim, J. H.; Lee, D. R.; Oh, C. S.; Yook, K. S.; Lee, J. Y. Recent Progress in High-Efficiency Blue-Light-Emitting Materials for Organic Light-Emitting Diodes. *Adv. Funct. Mater.* **2017**, *27*, 1603007. https://doi.org/10.1002/adfm.201603007.

(12) Xu, Z.; Tang, B. Z.; Wang, Y.; Ma, D. Recent Advances in High Performance Blue Organic Light-Emitting Diodes Based on Fluorescence Emitters. *J. Mater. Chem. C* **2020**, *8*, 2614–2642. https://doi.org/10.1039/c9tc06441a.

(13) Lee, J.-H.; Chen, C.-H.; Lee, P.-H.; Lin, H.-Y.; Leung, M.; Chiu, T.-L.; Lin, C.-F. Blue Organic Light-Emitting Diodes: Current Status, Challenges, and Future Outlook. *J. Mater. Chem. C* **2019**, *7*, 5874–5888. https://doi.org/10.1039/c9tc00204a.

(14) Li, W.; Pan, Y.; Xiao, R.; Peng, Q.; Zhang, S.; Ma, D.; Li, F.; Shen, F.; Wang, Y.; Yang, B. Employing ∼100% Excitons in OLEDs by Utilizing a Fluorescent Molecule with Hybridized Local and Charge-Transfer Excited State. *Adv. Funct. Mater.* **2014**, *24*, 1609–1614. https://doi.org/10.1002/adfm.201301750.

(15) Li, W.; Liu, D.; Shen, F.; Ma, D.; Wang, Z.; Feng, T.; Xu, Y.; Yang, B.; Ma, Y. A Twisting Donor-Acceptor Molecule with an Intercrossed Excited State for Highly Efficient, Deep-Blue Electroluminescence. *Adv. Funct. Mater.* **2012**, *22*, 2797–2803. https://doi.org/10.1002/adfm.201200116.

(16) Liu, Y.; Li, C.; Ren, Z.; Yan, S.; Bryce, M. R. All-Organic Thermally Activated Delayed Fluorescence Materials for Organic Light-Emitting Diodes. *Nature Rev. Mater.* **2018**, *3*, 18020. https://doi.org/10.1038/natrevmats.2018.20.

(17) Goushi, K.; Yoshida, K.; Sato, K.; Adachi, C. Organic Light-Emitting Diodes Employing Efficient Reverse Intersystem Crossing for Triplet-to-Singlet State Conversion. *Nature Photon.* **2012**, *6*, 253–258. https://doi.org/10.1038/nphoton.2012.31.

(18) Uoyama, H.; Goushi, K.; Shizu, K.; Nomura, H.; Adachi, C. Highly Efficient Organic Light-Emitting Diodes from Delayed Fluorescence. *Nature* **2012**, *492*, 234–238. https://doi.org/10.1038/nature11687.

(19) Zhang, Q.; Li, B.; Huang, S.; Nomura, H.; Tanaka, H.; Adachi, C. Efficient Blue Organic Light-Emitting Diodes Employing Thermally Activated Delayed Fluorescence. *Nature Photon.* **2014**, *8*, 326–332. https://doi.org/10.1038/nphoton.2014.12.

(20) Zhang, Q.; Li, J.; Shizu, K.; Huang, S.; Hirata, S.; Miyazaki, H.; Adachi, C. Design of Efficient Thermally Activated Delayed Fluorescence Materials for Pure Blue Organic Light Emitting Diodes. *J. Am. Chem. Soc.* **2012**, *134*, 14706–14709. https://doi.org/10.1021/ja306538w.

(21) Hirata, S.; Sakai, Y.; Masui, K.; Tanaka, H.; Lee, S. Y.; Nomura, H.; Nakamura, N.; Yasumatsu, M.; Nakanotani, H.; Zhang, Q.; Shizu, K.; Miyazaki, H.; Adachi, C. Highly Efficient Blue Electroluminescence Based on Thermally Activated Delayed Fluorescence. *Nature Mater.* **2015**, *14*, 330–336. https://doi.org/10.1038/nmat4154.

(22) Ward, J. S.; Kukhta, N. A.; dos Santos, P. L.; Congrave, D. G.; Batsanov, A. S.; Monkman, A. P.; Bryce, M. R. Delayed Blue Fluorescence via Upper-Triplet State Crossing from C–C Bonded Donor–Acceptor Charge Transfer Molecules with Azatriangulene Cores. *Chem. Mater.* **2019**, *31*, 6684–6695. https://doi.org/10.1021/acs.chemmater.9b01184.

(23) Zhang, D.; Cai, M.; Zhang, Y.; Zhang, D.; Duan, L. Sterically Shielded Blue Thermally Activated Delayed Fluorescence Emitters with Improved Efficiency and Stability. *Mater. Horiz.* **2016**, *3*, 145–151. https://doi.org/10.1039/c5mh00258c.

(24) Li, D.; Yuan, Y.; Bi, H.; Yao, D.; Zhao, X.; Tian, W.; Wang, Y.; Zhang, H. Boron-Bridged π-Conjugated Ladders as Efficient Electron-Transporting Emitters. *Inorg. Chem.* **2011**, *50*, 4825–4831. https://doi.org/10.1021/ic102554j.

(25) Wang, K.; Huang, S.; Zhang, Y.; Zhao, S.; Zhang, H.; Wang, Y. Multicolor Fluorescence and Electroluminescence of an ICT-Type Organic Solid Tuned by Modulating the Accepting Nature of the Central Core. *Chem. Sci.* **2013**, *4*, 3288. https://doi.org/10.1039/c3sc51091c.

(26) Zhang, Z.; Chen, Y.-A.; Hung, W.-Y.; Tang, W.-F.; Hsu, Y.-H.; Chen, C.-L.; Meng, F.-Y.; Chou, P.-T. Control of the Reversibility of Excited-State Intramolecular Proton Transfer (ESIPT) Reaction: Host-Polarity Tuning White Organic Light Emitting Diode on a New Thiazolo[5,4-d]Thiazole ESIPT System. *Chem. Mater.* **2016**, *28*, 8815–8824. https://doi.org/10.1021/acs.chemmater.6b04707.

(27) Bevk, D.; Marin, L.; Lutsen, L.; Vanderzande, D.; Maes, W. Thiazolo[5,4-*d*]Thiazoles – Promising Building Blocks in the Synthesis of Semiconductors for Plastic Electronics. *RSC Adv.* **2013**, *3*, 11418. https://doi.org/10.1039/c3ra40851e.

(28) Lin, Y.; Fan, H.; Li, Y.; Zhan, X. Thiazole-Based Organic Semiconductors for Organic Electronics. *Adv. Mater.* **2012**, *24*, 3087–3106. https://doi.org/10.1002/adma.201200721.

(29) Feng, Y.; Qiao, X.; Ouyang, G.; Liu, G.; Li, H. Thiazolothiazole-Based Quinoidal Compounds for High-Performance N-Channel Organic Field-Effect Transistors with Low-Cost Metal Electrodes. *Adv. Electron. Mater.* **2020**, *6*, 1901443. https://doi.org/10.1002/aelm.201901443.

(30) Schneider, J. A.; Black, H.; Lin, H.-P.; Perepichka, D. F. Polymorphism in New Thienothiophene-Thiazolothiazole Organic Semiconductors. *ChemPhysChem* **2015**, *16*, 1173–1178. https://doi.org/10.1002/cphc.201500066.

(31) Ando, S.; Nishida, J.; Tada, H.; Inoue, Y.; Tokito, S.; Yamashita, Y. High Performance N-Type Organic Field-Effect Transistors Based on π-Electronic Systems with Trifluoromethylphenyl Groups. *J. Am. Chem. Soc.* **2005**, *127*, 5336–5337. https://doi.org/10.1021/ja042219.

(32) Lim, D.-H.; Jang, S.-Y.; Kang, M.; Lee, S.; Kim, Y.-A.; Heo, Y.-J.; Lee, M.-H.; Kim, D.-Y. A Systematic Study on Molecular Planarity and D–A Conformation in Thiazolothiazole- and Thienylenevinylene-Based Copolymers for Organic Field-Effect Transistors. *J. Mater. Chem. C* **2017**, *5*, 10126–10132. https://doi.org/10.1039/c7tc02273e.

(33) Subramaniyan, S.; Xin, H.; Kim, F. S.; Shoaee, S.; Durrant, J. R.; Jenekhe, S. A. Effects of Side Chains on Thiazolothiazole-Based Copolymer Semiconductors for High Performance Solar Cells. *Adv. Energy Mater.* **2011**, *1*, 854–860. https://doi.org/10.1002/aenm.201100215.

(34) Dessì, A.; Calamante, M.; Sinicropi, A.; Parisi, M. L.; Vesce, L.; Mariani, P.; Taheri, B.; Ciocca, M.; Di Carlo, A.; Zani, L.; Mordini, A.; Reginato, G. Thiazolo[5,4-*d*]Thiazole-Based Organic Sensitizers with Improved Spectral Properties for Application in Greenhouse-Integrated Dye-Sensitized Solar Cells. *Sust. Energy Fuels* **2020**, *4*, 2309–2321. https://doi.org/10.1039/d0se00124d.

(35) Ameen, S.; Akhtar, M. S.; Nazim, M.; Nazeeruddin, M. K.; Shin, H.-S. Stable Perovskite Solar Cells Using Thiazolo [5,4-*d*]Thiazole-Core Containing Hole Transporting Material. *Nano Energy* **2018**, *49*, 372–379. https://doi.org/10.1016/j.nanoen.2018.04.016.

(36) Reginato, G.; Mordini, A.; Zani, L.; Calamante, M.; Dessì, A. Photoactive Compounds Based on the Thiazolo[5,4-*d*]Thiazole Core and Their Application in Organic and Hybrid Photovoltaics. *Eur. J. Org. Chem.* **2016**, *2016*, 233–251. https://doi.org/10.1002/ejoc.201501237.

(37) Peng, W.; Zhang, G.; Shao, L.; Ma, C.; Zhang, B.; Chi, W.; Peng, Q.; Zhu, W. Simple-Structured Small Molecule Acceptors Constructed by a Weakly Electron-Deficient Thiazolothiazole Core for High-Efficiency Non-Fullerene Organic Solar Cells. *J. Mater. Chem. A* **2018**, *6*, 24267–24276. https://doi.org/10.1039/c8ta09370a.

(38) Roy, I.; Bobbala, S.; Zhou, J.; Nguyen, M. T.; Nalluri, S. K. M.; Wu, Y.; Ferris, D. P.; Scott, E. A.; Wasielewski, M. R.; Stoddart, J. F. ExTzBox: A Glowing Cyclophane for Live-Cell Imaging. *J. Am. Chem. Soc.* **2018**, *140*, 7206–7212. https://doi.org/10.1021/jacs.8b03066.

(39) Woodward, A. N.; Kolesar, J. M.; Hall, S. R.; Saleh, N.-A.; Jones, D. S.; Walter, M. G. Thiazolothiazole Fluorophores Exhibiting Strong Fluorescence and Viologen-Like Reversible Electrochromism. *J. Am. Chem. Soc.* **2017**, *139*, 8467–8473. https://doi.org/10.1021/jacs.7b01005.

(40) Sayresmith, N. A.; Saminathan, A.; Sailer, J. K.; Patberg, S. M.; Sandor, K.; Krishnan, Y.; Walter, M. G. Photostable Voltage-Sensitive Dyes Based on Simple, Solvatofluorochromic, Asymmetric Thiazolothiazoles. *J. Am. Chem. Soc.* **2019**, *141*, 18780–18790. https://doi.org/10.1021/jacs.9b08959.

(41) Wang, K.; Zhang, H.; Chen, S.; Yang, G.; Zhang, J.; Tian, W.; Su, Z.; Wang, Y. Organic Polymorphs: One-Compound-Based Crystals with Molecular-Conformation- and Packing-Dependent Luminescent Properties. *Adv. Mater.* **2014**, *26*, 6168–6173. https://doi.org/10.1002/adma.201401114.

(42) Zhou, J.; Wu, Y.; Roy, I.; Samanta, A.; Stoddart, J. F.; Young, R. M.; Wasielewski, M. R. Choosing Sides: Unusual Ultrafast Charge Transfer Pathways in an Asymmetric Electron-Accepting Cyclophane That Binds an Electron Donor. *Chem. Sci.* **2019**, *10*, 4282–4292. https://doi.org/10.1039/c8sc05514a.

(43) Jouaiti, A.; Giuso, V.; Cebrián, C.; Mercandelli, P.; Mauro, M. Linear, Two- and Four-Armed Pyridine-Decorated Thiazolo[5,4-*d*]Thiazole Fluorophores: Synthesis, Photophysical Study and Computational Investigation. *Dyes and Pigments* **2022**, *208*, 110780. https://doi.org/10.1016/j.dyepig.2022.110780.

(44) Adhikari, R. M.; Mondal, R.; Shah, B. K.; Neckers, D. C. Synthesis and Photophysical Properties of Carbazole-Based Blue Light-Emitting Dendrimers. *J. Org. Chem.* **2007**, *72*, 4727–4732. https://doi.org/10.1021/jo0703911.

(45) Pinto, M. R.; Takahata, Y.; Atvars, T. D. Z. Photophysical Properties of 2,5-Diphenyl-Thiazolo[5,4-*d*]Thiazole. *J. Photochem. Photobiol. A: Chemistry* **2001**, *143*, 119–127. https://doi.org/10.1016/s1010-6030(01)00520-2.

(46) Cao, K.J.; Elbel, K. M.; Cifelli, J. L.; Cirera, J.; Sigurdson, C. J.; Paesani, F.; Theodorakis, E. A.; Yang, J. Solvation-guided design of fluorescent probes for discrimination of amyloids. *Sci. Rep.* **2018**, *8*, 6950. https://doi.org/10.1038/s41598-018-25131-2.

(47) Cao, K.; Farahi, M.; Dakanali, M.; Chang, W. M.; Sigurdson, C. J.; Theodorakis, E. A.; Yang, J. Aminonaphthalene 2-Cyanoacrylate (ANCA) Probes Fluorescently Discriminate between Amyloid-β and Prion Plaques in Brain. *J. Am. Chem. Soc.* **2012**, *134*, 17338–17341. https://doi.org/10.1021/ja3063698.

(48) Mataga, N.; Kaifu, Y.; Koizumi, M. The Solvent Effect on Fluorescence Spectrum, Change of Solute-Solvent Interaction during the Lifetime of Excited Solute Molecule. *Bull. Chem. Soc. Jpn.* **1955**, *28*, 690–691. https://doi.org/10.1246/bcsj.28.690.

(49) Lippert, E. Dipolmoment Und Elektronenstruktur von Angeregten Molekülen. *Zeit. für Naturforsch. A* **1955**, *10*, 541–545. https://doi.org/10.1515/zna-1955-0707.

(50) Wang, K.; Zhang, H.; Chen, S.; Yang, G.; Zhang, J.; Tian, W.; Su, Z.; Wang, Y. Organic Polymorphs: One-Compound-Based Crystals with Molecular-Conformation- and Packing-Dependent Luminescent Properties. *Adv. Mater.* **2014**, *26*, 6168–6173. https://doi.org/10.1002/adma.201401114.

(51) Ishi-i, T.; Tanaka, H.; Youfu, R.; Aizawa, N.; Yasuda, T.; Kato, S.; Matsumoto, T. Mechanochromic Fluorescence Based on a Combination of Acceptor and Bulky Donor Moieties: Tuning Emission Color and Regulating Emission Change Direction. *New J. Chem.* **2019**, *43*, 4998–5010. https://doi.org/10.1039/c8nj06050a.

(52) Li, D.; Zhang, Z.; Zhao, S.; Wang, Y.; Zhang, H. Diboron-Containing Fluorophores with Extended Ladder-Type π-Conjugated Skeletons. *Dalton Trans.* **2011**, *40*, 1279. https://doi.org/10.1039/c0dt01269f.

(53) Jou, J.-H.; Wang, W.-B.; Chen, S.-Z.; Shyue, J.-J.; Hsu, M.-F.; Lin, C.-W.; Shen, S.-M.; Wang, C.-J.; Liu, C.-P.; Chen, C.-T.; Wu, M.-F.; Liu, S.-W. High-Efficiency Blue Organic Light-Emitting Diodes Using a 3,5-Di(9*H*-Carbazol-9-Yl)Tetraphenylsilane Host via a Solution-Process. *J. Mater. Chem.* **2010**, *20*, 8411. https://doi.org/10.1039/c0jm01163k.

(54) Matsushima, H.; Naka, S.; Okada, H.; Onnagawa, H. Organic Electrophosphorescent Devices with Mixed Hole Transport Material as Emission Layer. *Curr. Appl. Phys.* **2005**, *5*, 305–308. https://doi.org/10.1016/j.cap.2003.11.091.

(55) Su, S.-J.; Chiba, T.; Takeda, T.; Kido, J. Pyridine-Containing Triphenylbenzene Derivatives with High Electron Mobility for Highly Efficient Phosphorescent OLEDs. *Adv. Mater.* **2008**, *20*, 2125–2130. https://doi.org/10.1002/adma.200701730.

(56) Ruduss, A.; Turovska, B.; Belyakov, S.; Stucere, K. A.; Vembris, A.; Baryshnikov, G.; Ågren, H.; Lu, J.-C.; Lin, W.-H.; Chang, C.-H.; Traskovskis, K. Thiazoline Carbene–Cu(I)–Amide Complexes: Efficient White Electroluminescence from Combined Monomer and Excimer Emission. *ACS Appl. Mater. Interfaces* **2022**, *14*, 15478–15493. https://doi.org/10.1021/acsami.2c00847.

(57) Lee, J.-H.; Cheng, S.-H.; Yoo, S.-J.; Shin, H.; Chang, J.-H.; Wu, C.-I.; Wong, K.-T.; Kim, J.-J. An Exciplex Forming Host for Highly Efficient Blue Organic Light Emitting Diodes with Low Driving Voltage. *Adv. Funct. Mater.* **2015**, *25*, 361–366. https://doi.org/10.1002/adfm.201402707.

(58) Yi, R.; Lei, Y.; Tseng, Y.; Lin, Y.; Cheng, Y.; Fang, Y.; Ho, C.; Tsai, W.; Chang, C.; Lu, C. Imidazolyl-Phenylcarbazole-Based Host Materials and Their Use for Co-host Designs in Phosphorescent OLEDs. *Chem. Eur. J.* **2022**, *28*, e202102966. https://doi.org/10.1002/chem.202102966.

(59) Yi, R.; Liu, G.; Luo, Y.; Wang, W.; Tsai, H.; Lin, C.; Shen, H.; Chang, C.; Lu, C. Dicyano-Imidazole: A Facile Generation of Pure Blue TADF Materials for OLEDs. *Chem. Eur. J.* **2021**, *27*, 12998–13008. https://doi.org/10.1002/chem.202101807.

(60) Lai, Y.-N.; Chang, C.-H.; Wang, P.-C.; Chu, Y.-H. Highly Efficient Flexible Organic Light-Emitting Diodes Based on a High-Temperature Durable Mica Substrate. *Org. Electr.* **2019**, *75*, 105442. https://doi.org/10.1016/j.orgel.2019.105442.

(61) Liao, C.-W.; Hsu, Y.-C.; Chu, C.-C.; Chang, C.-H.; Krucaite, G.; Volyniuk, D.; Grazulevicius, J. V.; Grigalevicius, S. Aggregation-Induced Emission Tetraphenylethene Type Derivatives for Blue Tandem Organic Light-Emitting Diodes. *Org. Electr.* **2019**, *67*, 279–286. https://doi.org/10.1016/j.orgel.2018.12.025.

(62) Dai, Y.; Zhang, H.; Zhang, Z.; Liu, Y.; Chen, J.; Ma, D. Highly Efficient and Stable Tandem Organic Light-Emitting Devices Based on HAT-CN/HAT-CN:TAPC/TAPC as a Charge Generation Layer. *J. Mater. Chem. C* **2015**, *3*, 6809–6814. https://doi.org/10.1039/c4tc02875a.

(63) Guo, Q.; Dai, Y.; Sun, Q.; Qiao, X.; Chen, J.; Zhu, T.; Ma, D. Properties of Highly Efficient Charge Generation and Transport of Multialternating Organic Heterojunctions and Its Application in Organic Light-Emitting Diodes. *Adv. Electron. Mater.* **2018**, *4*, 1800177. https://doi.org/10.1002/aelm.201800177.